AIP | Journal of Applied Physics

Enhanced infra-red emission from sub-millimeter microelectromechanical systems micro hotplates via inkjet deposited carbon nanoparticles and fullerenes

A. De Luca, M. T. Cole, A. Fasoli, S. Z. Ali, F. Udrea et al.

Citation: J. Appl. Phys. **113**, 214907 (2013); doi: 10.1063/1.4809546
View online: http://dx.doi.org/10.1063/1.4809546
View Table of Contents: http://jap.aip.org/resource/1/JAPIAU/v113/i21
Published by the American Institute of Physics.

JOURNAL OF APPLIED PHYSICS **113**, 214907 (2013)

Enhanced infra-red emission from sub-millimeter microelectromechanical systems micro hotplates via inkjet deposited carbon nanoparticles and fullerenes

A. De Luca,[1] M. T. Cole,[1,2] A. Fasoli,[1] S. Z. Ali,[2] F. Udrea,[1,2,a)] and W. I. Milne[1]
[1]*Department of Engineering, Electrical Engineering Division, University of Cambridge, 9 JJ Thomson Avenue, CB3 0FA Cambridge, United Kingdom*
[2]*Cambridge CMOS Sensors, St Andrew's House, Cambridge CB2 3BZ, United Kingdom*

(Received 11 March 2013; accepted 20 May 2013; published online 5 June 2013)

In this paper, we demonstrate a micro-inkjet printing technique as a reproducible post-process for the deposition of carbon nanoparticles and fullerene adlayers onto fully CMOS compatible micro-electro-mechanical silicon-on-insulator infrared (IR) light sources to enhance their infrared emission. We show experimentally a significant increase in the infrared emission efficiency of the coated emitters. We numerically validate these findings with models suggesting a dominant performance increase for wavelengths $<5.5\,\mu$m. Here, the bimodal size distribution in the diameter of the carbon nanoparticles, relative to the fullerenes, is an effective mediator towards topologically enhanced emittance of our miniaturised emitters. A 90% improvement in IR emission power density has been shown which we have rationalised with an increase in the mean thickness of the deposited carbon nanoparticle adlayer. © *2013 AIP Publishing LLC*. [http://dx.doi.org/10.1063/1.4809546]

I. INTRODUCTION

The demand for low-cost, high selectivity, low power consumption, and long life-time gas sensors has significantly increased over the past decade owing to the ubiquity of portable electronics devices. To date, electrochemical, catalytic, and metal-oxide gas sensors dominate the market. However, electrochemical sensors suffer from low life-times,[1] whilst poisoning,[2,3] and high power consumption[4] are key drawbacks of catalytic and metal-oxide technologies. In addition, temperature drift, poor long term stability, and very poor reproducibility of the metal-oxide are still issues to be addressed in spite of their reduced cost and enhanced sensitivity. Non-dispersive infra-red (NDIR) spectroscopic gas sensors are expensive,[5] largely due to system complexity, but offer high accuracy, high reliability, and enhanced selectivity.[1] Recently, much effort has been dedicated towards the development of low-cost, ultra-miniaturised NDIR systems.[6–10] Exploiting standard CMOS processes is an attractive route toward the fabrication of such infrared emitters and detectors. However, the emissive and absorptive properties of these devices often need to be modified to fulfill particular application requirements—such as gas species selectivity. Several solutions have been proposed including "black" coatings,[11,12] and quarter-wavelength structures,[13,14] in addition to plasmonic[15–20] and photonic crystal structures.[21–25] In this paper, we report on a reproducible post-process based on micro-inkjet deposition of graphitic carbon nanomaterial adlayers to augment the IR emissivity of fully CMOS compatible micro-electro-mechanical IR light sources, which we have theoretically and experimentally investigated. A 90% increase in the emitted IR radiation, primarily for wavelengths $<5.5\,\mu$m, has been shown which we have attributed to an enhanced optical coupling between the air and the heater passivation layer. Our work here suggests that this post-processing route is viable to enhance the signal-to-noise ratios for portable NDIR gas sensing systems, and thus, raises the possibility of unprecedented low gas concentration detection.

II. EXPERIMENT

The micro-IR optical emitter is shown in Figure 1(a) (Cambridge CMOS Sensors: CCS4_08_B). The structure was fabricated in a commercial foundry and was based on current-driven Joule heating micro-electro-mechanical silicon-on-insulator (SOI) technology (Fig. 1(b)), as reported in further detail elsewhere.[26,27] Briefly, a metal micro-heater is embedded within a $5\,\mu$m thick SiO_2 membrane ensuring low DC power consumption ($\leq$200 mW at 600 °C, Fig. 2(a)). The micro-hotplates can reach temperatures in excess to 700 °C, have a sub-5 V-controlled thermal ramp $>4 \times 10^4$ °C/s (Fig. 2(b)), and offers enhanced stability and reliability relative to micro-bulbs and other IR sources.[28] Membranes were fabricated via post CMOS deep reactive ion etching (DRIE), allowing the realization of near-vertical etch walls thereby reducing the required chip area consenting aggressive miniaturisation. The membrane mechanically supports, and thermally isolates, the micro-heater allowing fully integrated CMOS drivers to be located on-chip. The temperature profile (Fig. 2(c)) is almost constant across the heater (634 ± 3.8 °C) and decreases to ambient at the membrane-bulk substrate interface. The IR detector herein is a proprietary thermopile employing multiple serial thermocouples fabricated from silicon-on-insulator. The thermocouple hot junctions are embedded within a few micrometers of the SiO_2, whilst the cold junctions reside on the bulk Si substrate. The membrane ensures thermal isolation of the hot junctions thereby increasing the detector sensitivity. The

a)Author to whom correspondence should be addressed. Electronic mail: fu10000@cam.ac.uk

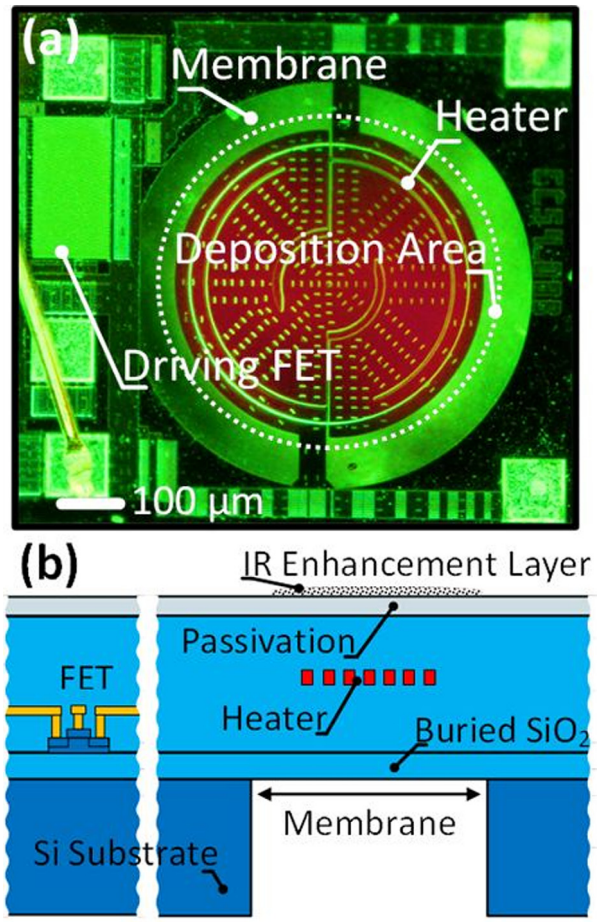

FIG. 1. MEMS SOI micro hotplate. (a) A UV-filtered optical micrograph of a typical bare micro hotplate (CCS4_08_B: Cambridge CMOS Sensors) radiating at 700 °C, featuring a 500 μm diameter heater embedded in a 700 μm diameter membrane. (b) Cross-section schematic depicting the MEMS SOI micro hotplate construction.

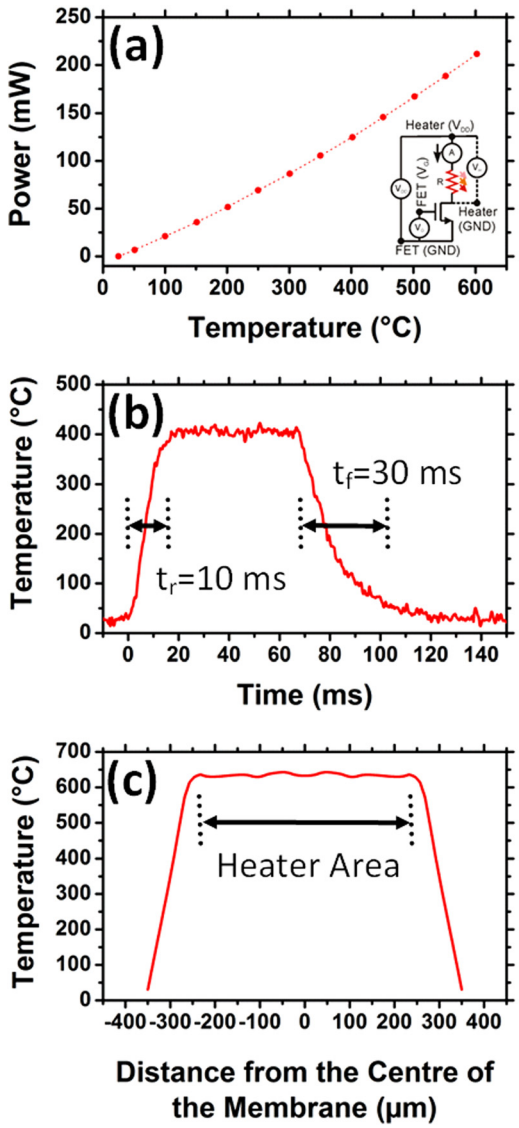

FIG. 2. Electro-thermal characterization. (a) Power dissipation as a function of heater temperature. Inset: Simplified circuit layout showing the micro hotplate driver. (b) Transient thermal behaviour (25–400 °C) showing a thermal rising time (10%-90%) of 10 ms and a thermal decay of 30 ms. (c) Simulated membrane temperature profile with a temperature ramp of 6 °C/μm in the membrane area.

thermopile output voltage is directly proportional to the number of thermocouples, the Seebeck coefficient, and the temperature difference between the substrate and membrane.

Carbon nanoparticle (CNPs, Sigma-Aldrich Ltd.: 633100) and C_{60} fullerene (Sigma-Aldrich Ltd.: 379646) adlayers were deposited, as-received, directly onto the sub-mm infra-red optical source by non-contact, ambient temperature micro-inkjet printing system (Autodrop Micro Dispensing System, Microdrop Tech.) fitted with a computer controlled piezo stage. Drop stability and the absence of satellite drops, which affected the measured reproducibility, were verified using a strobe MD-P-757 monitoring unit (Fig. 3(a)). Non-contact deposition ensured minimal damage to the membrane and highly accurate material deposition (Fig. 3(b)). The Raman spectra, shown in Fig. 3(c), were obtained using a Renishaw Raman spectrometer with an incident power of <3 mW, under 633 nm and 514 nm excitation. The C_{60} presents a typical strong pentagonal pinch mode at 1469 cm^{-1} and a $H_g(8)$ mode at 1580 cm^{-1},[29] while the CNPs show a D pick at 1360 cm^{-1} and the G pick at 1600 cm^{-1}. Drops had a nominal volume of approximately 10^2 pl. Samples were coated with $\sim 10^3$–10^5 drops. Suspensions of CNPs (0.05 mg/ml) and C_{60} (0.03 mg/ml) in isopropanol (IPA) were prepared. IPA was selected due to its low vapour pressure and temporally inhibited evaporation rate, which allowed reduction in tip dwell time between consecutive drop-streams which substantially improved material uniformity. To avoid settling within the as prepared suspensions, every 3 h suspensions were high-power sonicated (Diagenode Bioruptor UCD-200) for 5 min. It is important to highlight that the materials have been deposited not only on the passivation directly adjacent to the heater but also on the surrounding membrane to ensure spatially uniform emission enhancement. Note that the IR enhancing layer does not exceed the membrane edge, and does not provide a direct thermal bridge between the heater and the bulk Si substrate, as this would detrimentally increase power dissipation. Coated emitters were wedge bonded to Au plated TO5 packages (Fig. 3(d)) using 25.4 μm Au wire and a thermally conductive adhesive.

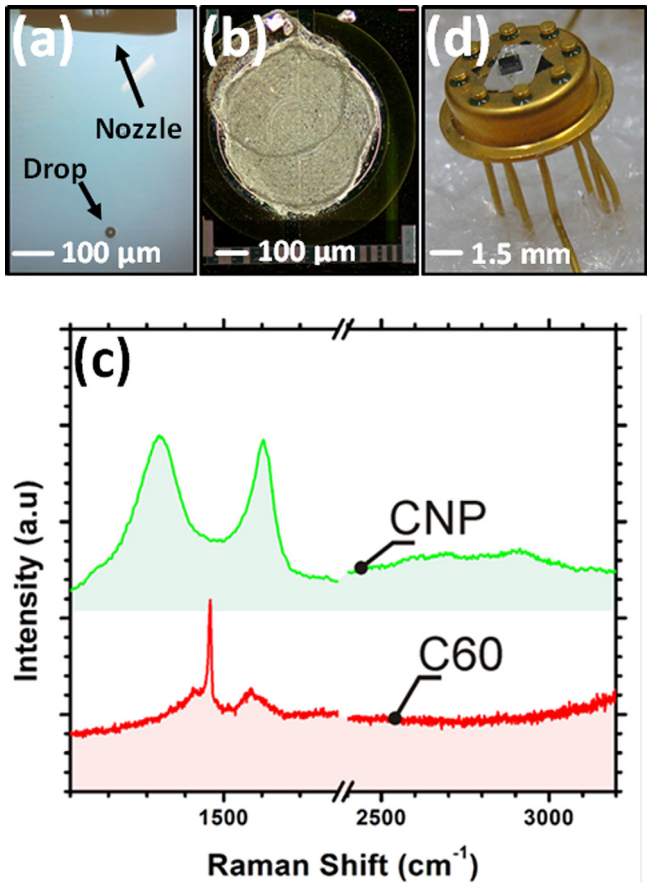

FIG. 3. Adlayer characterization: (a) Photograph of the inkjet printer nozzle during deposition (scale bar: 100 μm). (b) Optical micrograph of a typical device after CNPs deposition (scale bar: 100 μm). (c) Raman spectra (3 mW, 532 nm) CNP and C_{60}, post deposition. (d) Optical micrograph of a bonded augmented IR source on a TO5 package (scale bar: 1.5 mm).

The nanocarbon morphology (Figs. 4(a) and 4(b)) was determined using a Zeiss Gemini-Sigma and Philips XL 30 sFEG scanning electron microscopes. Distributions in nanoparticle diameter (Fig. 4(c)) were evaluated using the image analysis software, IMAGEJ. Absorbance and transmittance spectra (352–1088 nm) were obtained using quartz supports with an Ati-Unicam UV-Vis UV2 Spectrometer, and a Research Series FTIR (2.5–25.4 μm) using spectroscopic grade CsI (Fig. 5(a)).

The effect of the optical layer was evaluated by comparing coated emitters with bare devices (Fig. 6(a)) in a basic NDIR system. The NDIR setup consists of a metallic cylindrical cavity forming a 2.5 cm optical path (inset of Fig. 6(a)). All measurements were carried out at STP. An automated LABVIEW (v. 8.5) controlled Keithley 2400 Sourcemeter was used to drive the emitter, and after ~500 ms, a Keithley 2410 Sourcemeter was used to measure the detected voltage across the thermopile. Emission spectrum of bare IR sources was measured as function of emitter temperature (Fig. 6(b)), at STP, with a Perkin Elmer Frontier FTIR. Experimental results were corroborated independently via simulation (Fig. 6(c)).

In order to assess the temporal stability of the coating layers at high temperature, few mg of CNPs and C_{60} were deposited and annealed at 600 °C in air at STP and in Ar at

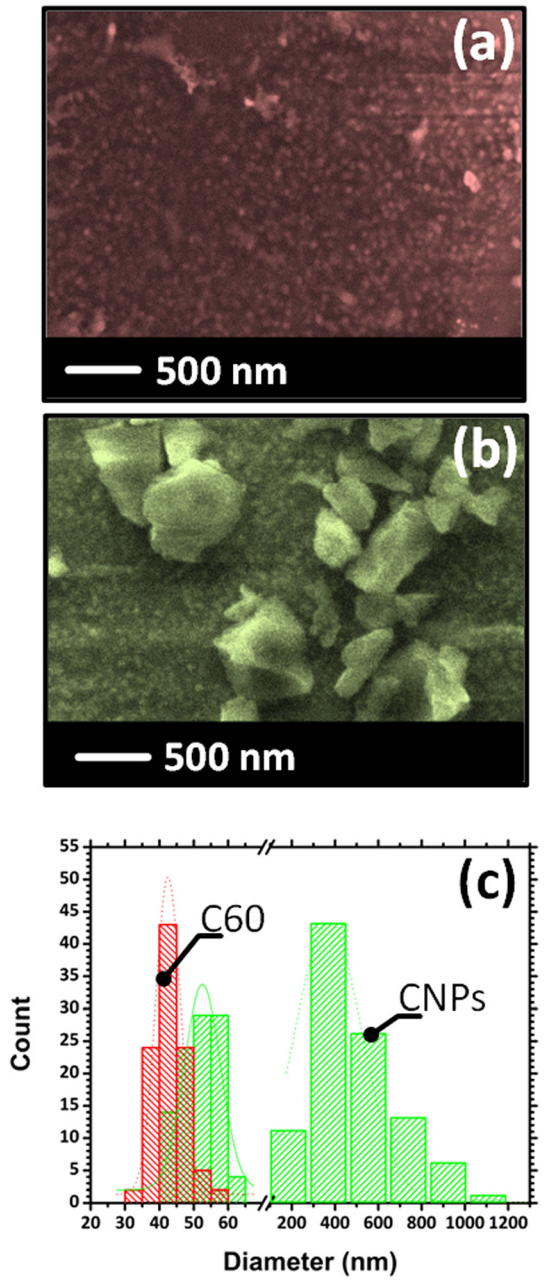

FIG. 4. Adlayer topological characterization: Scanning electron micrographs (false coloured) of an inkjet deposited (a) C_{60} film (scale bar: 500 nm) and (b) CNP film (scale bar: 500 nm). (c) CNPs (green) and C_{60} (red) diameter distributions.

1.25 mbar. The mass of the nanomaterials was periodically monitored using a microbalance (Fisherbrand, PS-200) located in a Terra Universal glove box to ensure accuracy.

III. RESULTS AND DISCUSSION

IR emitters are electro-thermo-optical transducers. They are electrically stimulated to deliver an optical output via heat. Electrical power is converted into thermal power, with the latter then being converted into optical power. This double transduction is performed via Joule-heating in a metallic or semiconductor resistor (in our case Tungsten), where the thermal output is partially dissipated through the membrane by conduction, and partially through the ambient via

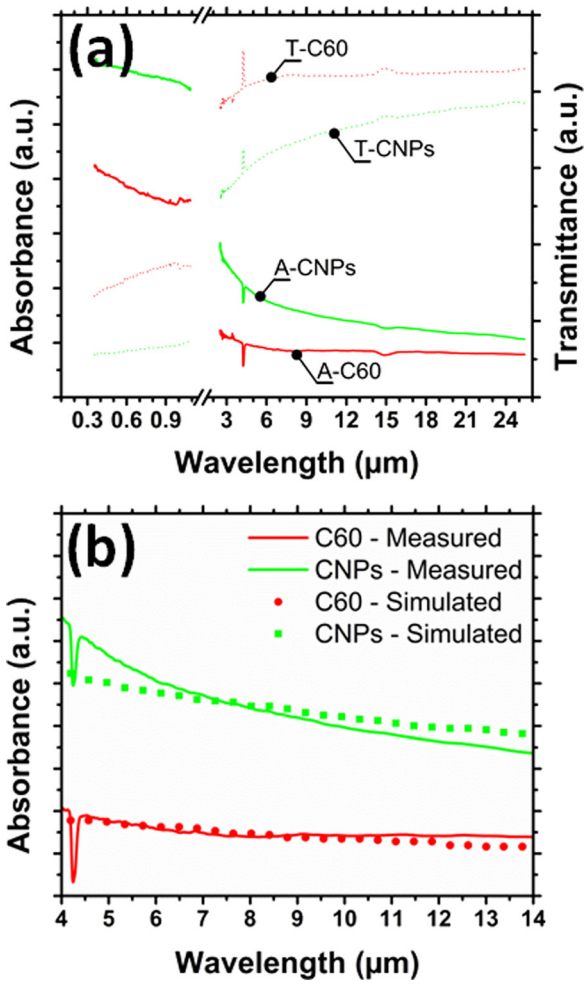

FIG. 5. IR emission augmentation: (a) Measured absorbance and transmittance of CNPs and C_{60} nanoparticles. (b) Comparison between experimental (solid line) and simulated (dotted line) absorbance for CNPs and C_{60} in the range of 4–14 μm.

convection. The remainder accounts for the functional and measureable optical component via radiation. The radiation is more prominent at higher temperatures and hence the need for temperatures in excess of 600 °C, to enhance the ratio between the useful radiative power versus the wasted power (convection and conduction). An IR detector performs the transduction in the opposite direction. The surface of the detector is thermally excited by the incident radiation with the thermopile converting the temperature into a proportional voltage. It is clearly shown in Fig. 6(a) that the coated emitters perform better than the bare ones. For instance, at 600 °C the thermopile voltage is enhanced by 30% in the case of a C_{60} adlayer, and 90% for a CNPs adlayer.

Bodies of finite, non-zero temperature emits IR at a characteristic wavelength.[30] The intensity of the radiation emitted by a black body (BB) is given by the Plank equation

$$I(\lambda,\ T) = \frac{2hc^2}{\lambda^5\left(e^{\frac{hc}{kT\lambda}} - 1\right)}, \qquad (1)$$

where T is the temperature of the BB, h is the Plank's constant, k is the Boltzmann's constant, c is the speed of light, and λ is the wavelength of the emitted radiation. BB are characterized by $\varepsilon = 1$, where ε is the emissivity. However, practically $\varepsilon < 1$. Such an emissivity is proper of grey bodies (GB) and is function of wavelength, temperature, surface

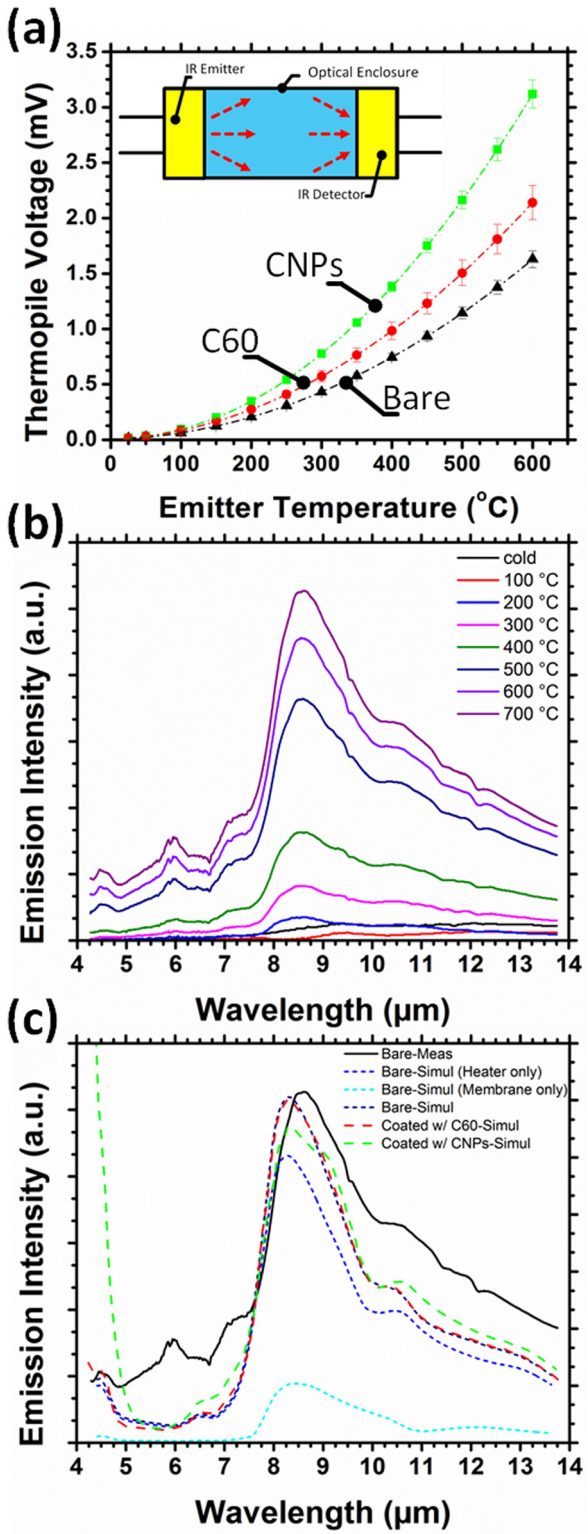

FIG. 6. Integrated and wavelength-dependent emission intensity. (a) Integrated intensity response due to adlayer introduction inferred from a thermopile voltage response as a function of emitter temperature. Inset: Schematic depiction of the NDIR setup. (b) Measured emission intensity as a function of wavelength at several emitter temperatures (from ambient to 700 °C). (c) Comparison between measured and simulated spectra for an emitter operating temperature of 700 °C. The modelled variation in emission due to the CNPs and C_{60} adlayers is also presented.

roughness, coating thickness, optical parameters, and topological and geometrical parameters.[31] As a consequence, the intensity of the radiation emitted by a GB, I_{GB}, is the BB intensity, I_{BB}, modulated by the emissivity: $I_{GB}(\lambda, T) = \varepsilon(\lambda, T, \ldots) \times I_{BB}(\lambda, T)$. According to Kirchhoff, at equilibrium for a given wavelength and temperature, the emittance of an object is equal to its absorbance: $\varepsilon = A = 1 - R - T$, where R is the reflectance and T is the transmittance.

The spectrum of a typical bare micro hotplate, at different working temperatures, is presented in Fig. 6(b). The emission spectrum is strongly affected by the non-ideal emittance of the multilayer stack, schematically depicted in Fig. 1(b). The majority of the emission occurs between 7 μm and 14 μm with a dominant peak at 8.6 μm, mainly due to the Si-O stretching vibration of the SiO_2 membrane.[32] This is a particularly attractive spectral feature for NDIR systems that target alcohol detection.[33] The experimental measurements are supported by simulation. An optical open source simulation package, which employs a matrix approach to derive the internal light absorption of the heater by calculating the light energy flux inside an approximate multilayer stack,[34] was used to estimate the wavelength-dependent absorbance of the bare micro hotplates between 4 μm and 14 μm, at normal incidence. This 1D modelling approach is justified since the membrane thickness is much smaller than its diameter. Optical constants (at STP) of the materials employed were taken from Palik[35] and Yin and Smith.[36] The intensity of the emitted radiation was obtained assuming a constant temperature of 700 °C in the heater area and a linearly decreasing temperature profile, from 700 °C to 25 °C, in the membrane area. Two different absorbance functions and geometrical dimensions were also considered for the heater and for the membrane area. If we take into account the broadening of the absorption peak, as reported here,[37] good agreement between theoretical and experimental data has been obtained (Fig. 6(c)). It is worth mentioning that the non-negligible contribution to the emissions generated by the membrane comes at zero power consumption.

Further simulations were carried out to evaluate the effect of the CNPs and C_{60} enhancing layers on the emission spectra. The Raman spectra (Fig. 3(c)) confirm the graphitic nature of the CNPs and C_{60}. Thus, graphitic optical properties, taken from Maron,[38] were used for both. SEM analysis (Figs. 4(a) and 4(b)) showed that the C_{60} dispersions were characterized by a monomodal size distribution with a mean diameter of 43 ± 5 nm, whereas the CNPs had a bimodal distribution consisting of small C_{60}-like particles (51 ± 5 nm) with much larger agglomerates (426 ± 204 nm) (Fig. 4(c)). Thus, in the simulations, an average thickness of 40 nm was considered for the C_{60} IR enhancing layer, and an average thickness of 200 nm for the CNP layer. In order to verify the validity of the material models (optical properties and thickness), the absorbance of C_{60} fullerenes and CNPs was experimentally measured (Fig. 5(a)). The results show an increase of the absorbance moving towards low wavelengths. The peaks at 4.25 μm and 15.0 μm are attributed to CO_2 asymmetric stretching and bending vibrations,[39] respectively. In Fig. 5(b), agreement between experimental and theoretical data is reported between 4 and 14 μm. The CNPs layer has a higher absorbance relative to the C_{60} layer due to its higher mean thickness, as postulated by Beer-Lambert. In Fig. 6(b), the theoretical effect of CNPs and C_{60} adlayers on the IR emissions is also presented. The presence of the IR enhancing layer strongly affect the emission power density for $\lambda < 5.5$ μm. Hence, we believe that coated emitters significantly improve the S/N ratio of NDIR systems targeting CO_2 detection.

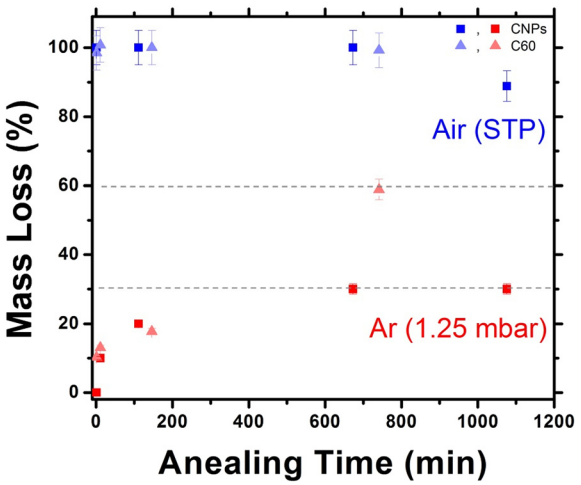

FIG. 7. Adlayer temporal stability. CNP and C_{60} adlayer temporal stability at 600 °C in air at STP and Ar at 1.25 mbar.

Fig. 7 shows the temporal stability of a CNPs and C_{60} adlayers stressed at 600 °C. When annealed in air at ambient pressure, carbon reacts with oxygen and the adlayer almost completely (>97%) etches rapidly (<1 min). When annealed in an Ar atmosphere at low pressure (1.25 mbar), the CNP adlayer showed an improved temporal stability which stabilises to around a 30% mass loss (of the original deposited adlayer mass) in a 10%–90% rise-time of 530 min continuous operation. On the contrary, the mass loss saturation of the C_{60} nanoparticles did not tend to saturate and was approximately 60% after 700 min DC operation. IR emitters are often hermetically sealed in low pressure, inert atmospheres with optical filtering windows, in order (i) to improve the selectivity of the NDIR system and to filter out unwanted radiated wavelengths; (ii) avoid interaction with oxygen, and thus, evaporation and/or oxidization; and (iii) to dramatically reduce thermal convection losses, thereby significantly improving the electro-thermal conversion efficiency. Another important consideration is that the same coatings can be employed to enhance the absorption of IR detectors, such as thermopiles, which work at ambient temperature and do not suffer from such temporal stability problems. We have also found that other graphitic nanocarbons, namely, CNTs, have proven to be stable for up to 100 h continuous operation at 500 °C in air.

IV. CONCLUSIONS

In this paper, the performances of carbon nanoparticle and fullerene IR emitting adlayers deposited via micro-inkjet printing have been investigated. Inkjet printing has shown to be a reproducible post process technique that is well-suited

for fragile MEMS devices. Raman spectroscopy, scanning electron microscopy, UV-Vis and FTIR spectroscopy were employed for the material characterization. FTIR spectroscopy was also used for the optical characterization of the bare infra-red light sources, in addition to the optical analysis carried out with basic NDIR system, for both coated and uncoated emitters. Experimental results were corroborated by simulations which suggested a strong peak in the emissions at 8.6 μm, making them very attractive for alcohol detection. CNPs increase the emission intensity by 90%, which was significant compared to the C_{60} fullerenes, which elicited a 30% improvement. Simulations predicted a dominant enhancement for wavelengths <5.5 μm. We believe that the nano-scale topological adjustment in the emission performance significantly improves the signal-to-noise ratio of NDIR systems for CO_2 detection and is very encouraging towards the realization for inexpensive, low power consuming, and truly mobile NDIR systems.

ACKNOWLEDGMENTS

M.T.C acknowledges the generous financial support of the Isaac Newton Trust, Trinity College Cambridge, and the Winston Churchill Trust. This work was partly supported through the EU FP7 projects: GRAFOL (2852754) and SOI-HITS (288481).

[1]J. Chou, *Hazardous Gas Monitors: A Practical Guide to Selection, Operation and Applications* (McGraw-Hill & SciTech Publishing, 1999).
[2]S. J. Gentry and P. T. Walsh, Sens. Actuators **5**, 229 (1984).
[3]J. Kwon, G. Ahn, G. Kim, J. C. Kim, and H. Kim, in *Proceedings of 2009 ICCAS-SICE* (Fukuoka, 2009), p. 1683.
[4]J. W. Gardner, *Microsensors, MEMS, and Smart Devices* (John Wiley & Sons Ltd, 2002).
[5]T. Stolberg-Rohr, R. Buchner, A. Krishna, L. Munch, K. Pihl, J. S. Hansen, S. Tojaga, H. G. Moos, and J. M. Jensen, in *2011 IEEE Sensors* (Limerick, 2011), p. 1058.
[6]C. Calaza, M. Salleras, N. Sabaté, J. Santander, C. Cané, and L. Fonseca, Microsyst. Technol. **18**, 1147 (2012).
[7]K. Qian, F. Li, H. San, and X. Chen, in 5th IEEE International Conference on Nano/Micro Engineered and Molecular Systems, Xiamen, China (2010).
[8]H. Sana, X. Chena, M. Chenga, and F. Lia, Proc. SPIE **6836**, 68360N-1 (2007).
[9]C. Calaza, E. Meca, S. Marco, M. Moreno, J. Samitier, L. Fonseca, I. Gracia, and C. Cane, in *Proceedings of IEEE Sensors* (2002), Vol. 2, p. 1323.
[10]H. Wu, A. Emadi, G. de Graaf, and R. F. Wolffenbuttel, Proc. SPIE **7726**, 772612 (2010).
[11]W. Lang, K. Kuhl, and H. Sandmaier, Sens. Actuators, A **34**, 243 (1992).
[12]N. Nelms and J. Dowson, Sens. Actuators, A **120**, 403 (2005).
[13]A. D. Parsons and D. J. Pedder, J. Vac. Sci. Technol. A **6**, 1686 (1988).
[14]P. Eriksson, J. Y. Anderson, and G. Stemme, Phys. Scr. **T54**, 165 (1994).
[15]C.-Y. Chen, M.-W. Tsai, Y.-W. Jiang, Y.-H. Ye, and Y.-T. Chang, Appl. Phys. Lett. **91**, 243111 (2007).
[16]C.-M. Wang and Y.-C. Chang, Opt. Express **15**, 14673 (2007).
[17]K. Ikeda, H. T. Miyazaki, T. Kasaya, K. Yamamoto, and Y. Inoue, Appl. Phys. Lett. **92**, 021117 (2008).
[18]Y.-W. Jiang, M.-W. Tsai, Y.-H. Ye, D.-C. Tzuang, C.-Y. Chen, and S.-C. Lee, in *Nanotechnology, 2008. NANO '08. 8th IEEE Conference on* (2008), pp. 104.
[19]S.-Y. Huang, P.-E. Chang, H.-H. Chen, C.-H. Chen, C.-W. Yu, and S.-C. Lee, in *11th IEEE International Conference on Nanotechnology, Portland Marriott* (2011), p. 1267.
[20]F. Li, H. San, C. Li, Y. Li, and X. Chen, J. Micromech. Microeng. **21**, 105023 (2011).
[21]X. Ji, X. Zhao, P. Jing, F. Xing, and Y. Huang, in 2010 10th IEEE International Conference on Solid-State and Integrated Circuit Technology (ICSICT), Shanghai (2010).
[22]I. Puscasu, E. Johnson, A. Taylor, B. Schell, W. Schaich, and R. Biswas, in *MRS Proceedings* (Cambridge University Press, 2009), Vol. 1162, pp. 1162.
[23]D. L. C. Chan, M. Soljacic, and J. D. Joannopoulos, Opt. Express **14**, 8785 (2006).
[24]V. Shklover, L. Braginsky, G. Witz, M. Mishrikey, and C. Hafner, J. Comput. Theor. Nanosci. **5**, 862 (2008).
[25]M. De Zoysa, T. Asano, K. Mochizuki, A. Oskooi, T. Inoue, and S. Noda, Nature Photon. **6**, 535–539 (2012).
[26]S. Z. Ali, F. Udrea, W. I. Milne, J. W. Gardner, J. Park, and S. Maeng, IEEE J. Microelectromech. Syst. **17**, 1408 (2008).
[27]F. Udrea, S. Maeng, J. W. Gardner, J. Park, M. S. Haque, S. Z. Ali, Y. Choi, P. K. Guha, S. M. C. Vieira, H. Y. Kim, K. C. Kim, S. E. Moon, K. H. Park, W. I. Milne, and S. Y. Oh, in *IEEE International Electron Devices Meeting, IEDM, Washington DC, USA* (2007), p. 831.
[28]F. Udrea, S. Z. Ali, M. Brezeanu, V. Dumitru, O. Buiu, I. Poenaru, M. F. Chowdhury, A. De Luca, and J. W. Gardner, in 2012 International Semiconductor Conference (CAS), Sinaia, Romania (2012).
[29]H. Kuzmany, R. Pfeiffer, M. Hulman, and C. Kramberger, Philos. Trans. R. Soc. London **362**, 2375 (2004).
[30]M. Plank, *The Theory of Heat Radiation* (Philadelphia, P. Blakiston's Son & Co, 1914).
[31]X. He, Y. Li, L. Wang, Y. Sun, and S. Zhang, Thin Solid Films **517**, 5120 (2009).
[32]M. Klevenz, S. Wetzel, M. Moller, and A. Pucci, Soc. Appl. Spectrosc. **64**, 298 (2010).
[33]J. J. Harrison, N. D. C. Allen, and P. F. Bernath, J. Quant. Spectrosc. Radiat. Transf. **113**, 2189 (2012).
[34]E. Centurioni, Appl. Opt. **44**, 7532 (2005).
[35]E. D. Palik, *Handbook of Optical Constants of Solids* (Academic Press, 1998).
[36]Z. Yin and F. W. Smith, Phys. Rev. B **42**, 3666 (1990).
[37]E. Cozzani, C. Summonte, L. Belsito, G. C. Cardinali, and A. Roncaglia, in *IEEE Sensors* (2007), p. 181.
[38]N. Maron, Astrophys. Space Sci. **172**, 21 (1990).
[39]R. A. Nyquist, *Interpreting Infrared, Raman and Nuclear Magnetic Resonance Spectra* (Academic Press, 2001).